ELSEVIER

Earth and Planetary Science Letters 174 (1999) 173–181

EPSL

www.elsevier.com/locate/epsl

Extraction of a lithospheric cooling signal from oceanwide geoid data

John DeLaughter [a], Seth Stein [b,*], Carol A. Stein [c]

[a] *Chevron Petroleum Technology Company, San Ramon, CA 94583, USA*
[b] *Department of Geological Sciences, Northwestern University, Evanston, IL 60208, USA*
[c] *Department of Earth and Environmental Sciences, University of Illinois at Chicago, Chicago, IL 60607-7059, USA*

Received 4 January 1999; received in revised form 16 August 1999; accepted 8 October 1999

Abstract

The geoid, an equipotential surface of Earth's gravity field, reflects the distribution of mass within the planet and hence a variety of geodynamic processes. Because these data are dominated by sublithospheric processes, notably mantle convection, they have not played a major role in the ongoing debate concerning models of the thermal evolution of oceanic lithosphere. Application of spatial filtering to the age derivative of the geoid, however, extracts an age-dependent signal which reflects lithospheric thermal evolution. The data are much better fit by a thin (about 100 km thick) thermal plate than by a cooling halfspace, and so provide a valuable constraint complementary to and consistent with the variations in oceanic depth and heat flow with age.

Keywords: geoid; lithosphere; thermal history; plate tectonics

1. Introduction

A remarkable feature of Earth's gravity field is that its major features bear little resemblance to the near-surface features of mantle convection expressed at the surface by plate tectonics, the primary mode of heat transfer from Earth's interior [1], which makes Earth's tectonics so different from our neighboring planets [2]. This difficulty is shown by comparison of Fig. 1A, a global map of lithospheric ages [3], to Fig. 1B, showing geoid anomalies, the deviation of the sealevel equipotential surface of gravity from the ellipsoidal shape of a rotating Earth [4]. The geoid anomalies are dominated by long wavelength features [5] interpreted as largely reflecting deep mantle convection [6,7]. Although some effects of subducting slabs are visible, there is little correspondence between the distribution of lithospheric age and the geoid. Hence oceanic spreading centers and the resulting cooling of oceanic lithosphere as it moves toward subduction zones are not obvious in the geoid, although this cooling is evident from the increase in ocean depths and decrease in seafloor heat flow with lithospheric age [8–11].

In theory, cooling of the lithosphere should cause the geoid to vary with age, as it reflects the integral of the thermal density anomaly

* Corresponding author. Tel.: +1-847-491-5265; Fax: +1-847-491-8060; E-mail: seth@earth.nwu.edu

0012-821X/99/$ – see front matter
PII: S0012-821X(99)00247-2

weighted by the depth, and thus the weighted integral of the geotherm. Hence geoid data should be valuable in the ongoing debate about how best to model thermal evolution of oceanic lithosphere. Because temperatures at depth are not directly measurable, this issue is generally addressed via models which seek to provide a simple description of the average thermal structure as a function of age. Traditionally, the primary surface observables constraining these models are variations in seafloor depth and heat flow with lithospheric age. In the models, seafloor depth depends on temperature integrated through the lithosphere, whereas heat flow depends on the temperature gradient at the seafloor.

The simplest such model is one in which the lithosphere evolves as the upper boundary layer of a cooling halfspace as it moves away from midocean ridges. This model describes the observation that depth and heat flow vary approximately with the square root of lithospheric age [9]. However, for ages older than about 70 Myr depth and heat flow 'flatten', varying more slowly with age than for a halfspace. It is thus generally assumed that halfspace cooling is perturbed by additional heat from below, which balances the heat lost at the seafloor, stops the lithosphere from continuing to cool for older ages, and thus causes flattening. The plate model, a simple and common description for this perturbation, uses an isothermal boundary at the base of the lithosphere to model the thermal equilibration of old lithosphere [12,13]. The plate model fits the data reasonably well, but does not directly describe how the heat is added from below [14–16]. Although the plate and halfspace models are the same for young ages, the two models make different predictions for ages old enough that the basal condition has an effect.

Until recently, it was common to use a model of a 125 km thick plate (denoted here PSM), following Parsons and Sclater's [17] demonstration that such a model described depths and heat flow for old ages better than a halfspace. However, this model still systematically overpredicts depths and underpredict heat flow for lithosphere older than 70–100 Myr, giving rise to widespread apparent depth and heat flow 'anomalies' [18]. This situation prompted a recent joint inversion of the depth and heat flow data [18], which found that these 'anomalies' are reduced significantly by the best-fitting plate model, termed GDH1. GDH1 is characterized by a plate with an asymptotic thermal thickness of 95 ± 10 km, thinner than the previously estimated 125 ± 10 km thick plate, and a basal temperature of 1450 ± 100°C, consistent with the previous estimate of 1350 ± 275°C [17]. Subsequent analyses showed that various depth and heat flow data not inverted in deriving GDH1 [19–22] were also better fit by the thin-lithosphere model than by the thick-lithosphere PSM model or by a halfspace model (which can be viewed as an infinitely thick plate). A thinner plate results even if the basal temperature is fixed in the inversions. For example, inverting the data from [18] assuming a fixed basal temperature of 1350°C yields a model (GDH1A) with a 100 km thick plate, a coefficient of thermal expansion of 3.1×10^{-5} K^{-1}, and thermal conductivity 3.65 W m^{-1} $°C^{-1}$. These parameters predict depth, heat flow, and geoid slope variations with age very similar to those for GDH1.

In view of these results, we refined our analysis [23] using newer global bathymetric [24], age [3], and sediment thickness data [25], and again find that the thinner thermal plate appears to be a robust result. For the depth data, hotspot swells were removed using the geoid-topography ratio filter discussed later in this paper. Inverting these data using the same method as [18] but with basal

→

Fig. 1. Successive stages in the data processing sequence. We seek the effect of lithospheric cooling, which should cause geoid anomalies dependent on lithospheric age (A). We begin with the unfiltered geoid (B), which shows little relation to lithospheric age, but is instead dominated by long-wavelength features interpreted as largely reflecting deep mantle convection. We then apply a bandpass filter to the data (C), and then take the slope of the bandpassed data in the direction of increasing age (D). These data are visually somewhat similar to the age data, showing both spreading centers and a general variation with age. To remove the effect of hotspot swells, we use a window function based on the gradient of the ratio of geoid to topography (E), and exclude values greater than 5 mm km^{-2}. The resulting data (F) show a clear average variation with lithospheric age.

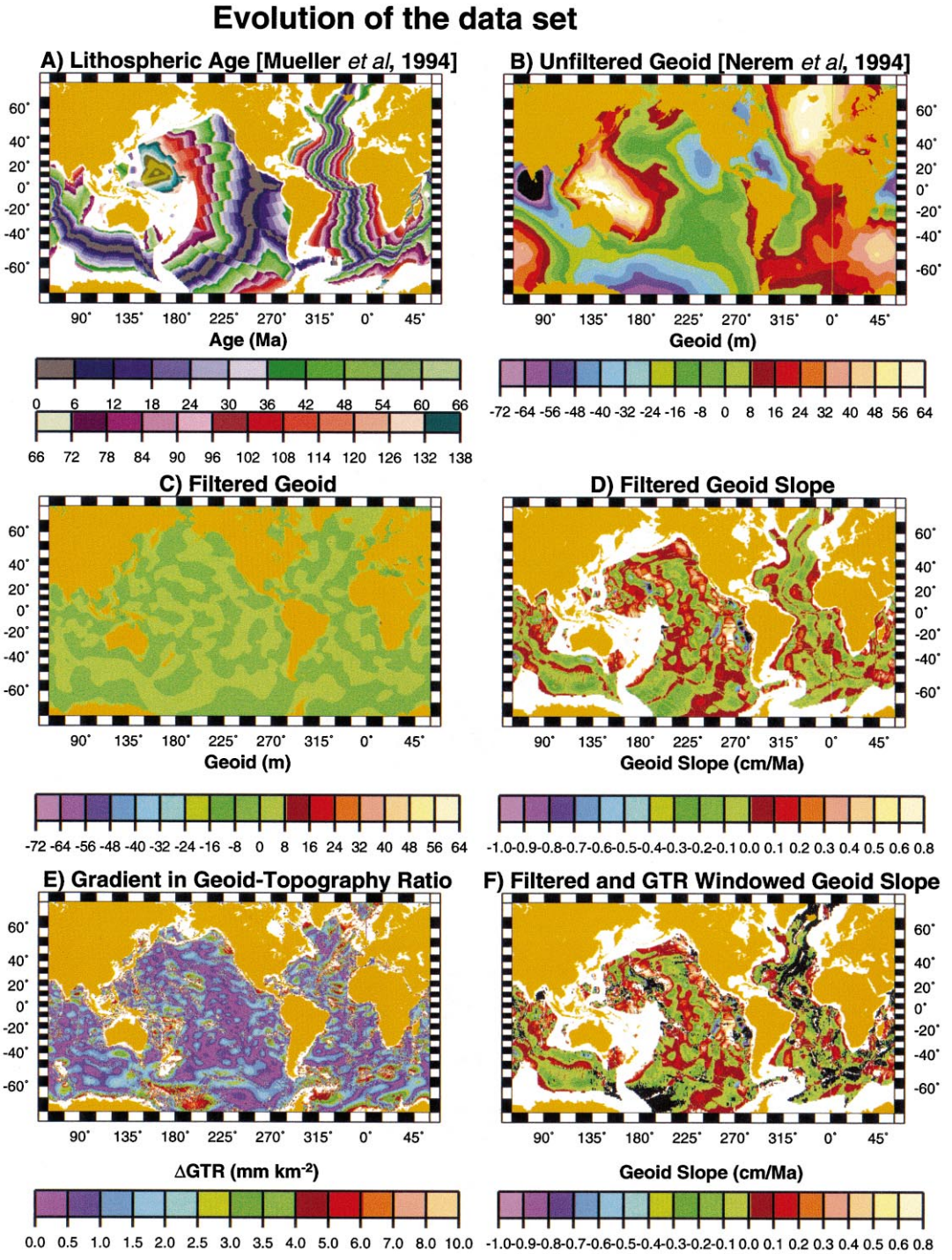
Evolution of the data set
A) Lithospheric Age [Mueller et al, 1994]
B) Unfiltered Geoid [Nerem et al, 1994]
60° 40° 20° 0° -20° -40° -60°
90° 135° 180° 225° 270° 315° 0° 45°
Age (Ma)
0 6 12 18 24 30 36 42 48 54 60 66
66 72 78 84 90 96 102 108 114 120 126 132 138
Geoid (m)
-72 -64 -56 -48 -40 -32 -24 -16 -8 0 8 16 24 32 40 48 56 64
C) Filtered Geoid
D) Filtered Geoid Slope
Geoid (m)
-72 -64 -56 -48 -40 -32 -24 -16 -8 0 8 16 24 32 40 48 56 64
Geoid Slope (cm/Ma)
-1.0 -0.9 -0.8 -0.7 -0.6 -0.5 -0.4 -0.3 -0.2 -0.1 0.0 0.1 0.2 0.3 0.4 0.5 0.6 0.8
E) Gradient in Geoid-Topography Ratio
F) Filtered and GTR Windowed Geoid Slope
ΔGTR (mm km-2)
0.0 0.5 1.0 1.5 2.0 2.5 3.0 3.5 4.0 5.0 6.0 7.0 8.0 10.0
Geoid Slope (cm/Ma)
-1.0 -0.9 -0.8 -0.7 -0.6 -0.5 -0.4 -0.3 -0.2 -0.1 0.0 0.1 0.2 0.3 0.4 0.5 0.6 0.8

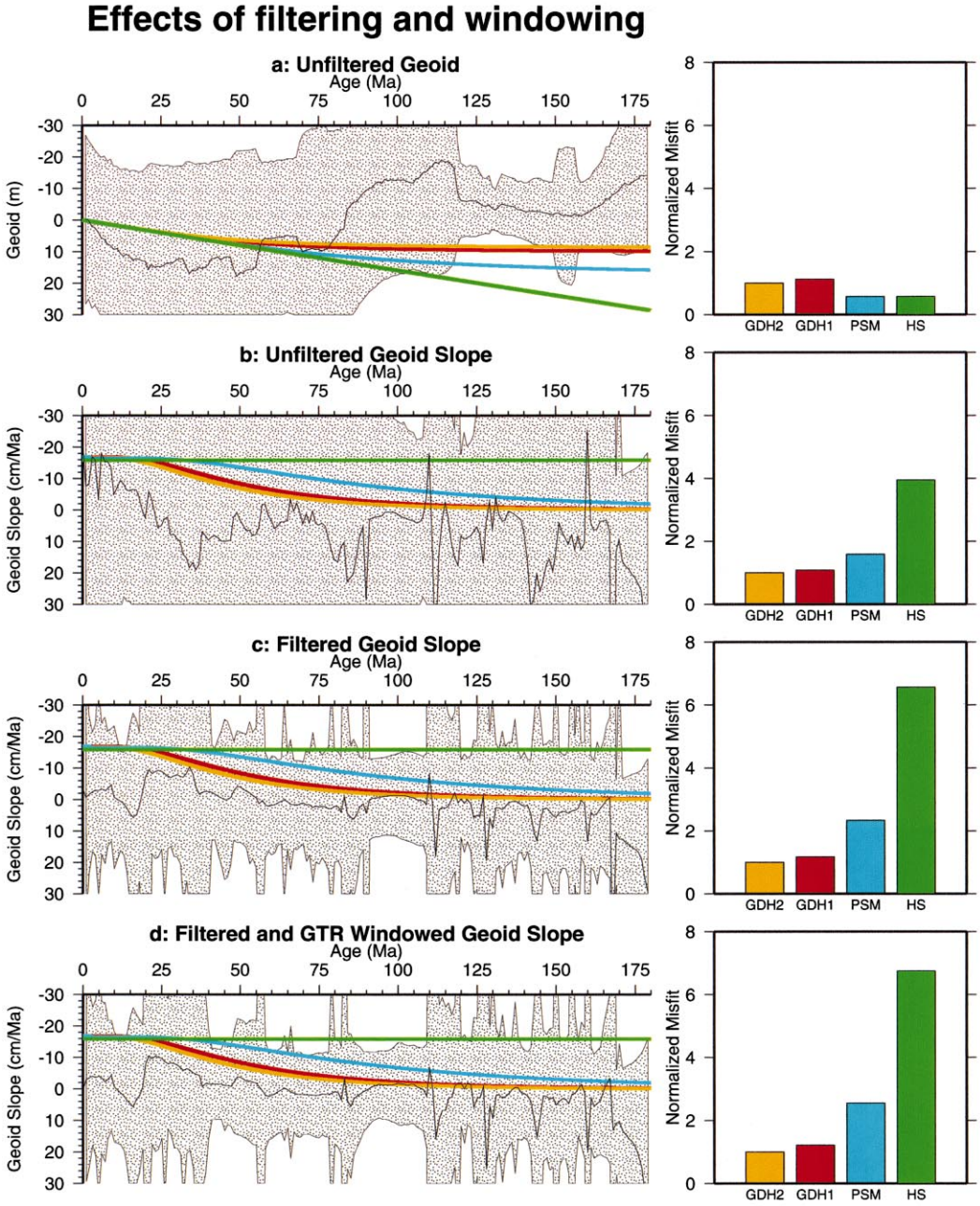

Fig. 2. Effect of successive stages in the data processing sequence on the extraction of the expected lithospheric cooling signal, which should cause geoid anomalies to vary with age. For each stage, data in 1 min grids are shown, together with the mean values. Also shown are predictions of thermal models: cooling halfspace (HS), thick-plate (PSM), and thin-plate models (GDH1, GDH2). Model misfits to data for each stage are normalized by the GDH2 misfit. The unfiltered geoid (a) shows few effects of lithospheric age, and so is poorly fit by all models. At each of the successive stages (Fig. 1) the data mean shows the expected age-dependent signal more clearly, and permits resolution between lithospheric cooling models. The data are better fit by the two thin-plate models (GDH1, GDH2) than by the thicker-plate (PSM) or halfspace (HS) models.

temperature fixed to 1350°C yields best fitting parameters for the plate thickness (90 km), coefficient of thermal expansion (3.1×10^{-5} K^{-1}), and thermal conductivity (3.25 W m^{-1} $°C^{-1}$). This inversion result, termed GDH2, is similar to GDH1, with GDH2 depths somewhat shallower compared to GDH1. At 180 Myr, GDH2 predicts depths about 350 m shallower than GDH1. This difference is because the GDH2 depth data come from all oceans, rather than only the northwest Atlantic and northern Pacific oceans used in the GDH1 data set. Subsequent to [18] analyses show that the other oceans are typically shallower at older ages (e.g., [21]).

2. Prior analyses with geoid data

Although geoid data should be applicable to study lithospheric evolution, doing so has proved challenging. The expected signal associated with plate cooling should be small, because it reflects processes in only the upper hundred or so km of a 2900 km thick mantle, a difficulty compounded by the fact that the geoid is most affected by density anomalies at depth [8]. Efforts to extract a plate cooling signal from geoid data have thus relied on taking the geoid slope, the gradient of the geoid in the direction of increasing lithospheric age, to reduce the long wavelength components. Geoid slope (Fig. 2b) should be constant with age for a halfspace model with a value proportional to the product of the melting temperature at the ridge and the coefficient of thermal expansion [9]. For a plate model, the predicted slope is the same as for a halfspace at young ages, but 'rolls off' at older ages at a rate depending inversely on the plate thickness [10] (Table 1). This effect is similar to the 'flattening' of the ocean depth and heat flow, in that these deviations from the square-root-of-age variation predicted by a halfspace model are expected if the lithosphere approaches an equilibrium thickness at older ages.

Table 1
Constraints on thermal models

Observable	Proportional to	Reflects
Young ocean depth	$\int T(z,t)\ dz$	αT_m
Old ocean depth	$\int T(z,t)\ dz$	$\alpha T_m a$
Old ocean heat flow	$\frac{\partial T(z,t)}{\partial z}\vert_{z=0}$	T_m/a
Geoid slope	$\frac{\partial}{\partial t}\int zT(z,t)\ dz$	$\alpha T_m \exp(-t/a^2)$

Plate thickness (a), basal temperature (T_m), coefficient of thermal expansion (α).
Halfspace model corresponds to $a\rightarrow\infty$.

Attempts to extract this age-dependent geoid slope signal from geoid data have followed two approaches. The most common has been to estimate geoid slope from the change in the geoid across fracture zones, which juxtapose lithosphere of two different ages [8,10,26–32]. The difficulty is that in addition to the thermal effect of the age contrast, the signal includes both a long-wavelength component (presumably reflecting deep sublithospheric mantle flow) and a shorter-wavelength component, which may reflect flexural and other effects at the fracture zone [33–35]. As a result, such studies yield scattered results. Taken collectively, these data are better (though far from perfectly) fit by a plate model with a thin (95 km) lithosphere than by either a halfspace or a 125 km thick plate [32], in accord with depth and heat flow data [18–22]. However, the scatter in the data, and a systematic misfit at young ages, make the agreement of the thin-plate model less than fully convincing.

An alternative approach is to estimate geoid slope directly from oceanwide geoid data. Unfortunately, although geoid slope is easily estimated near ridges [36,37], it proved harder to obtain consistent estimates for older ages, so this technique has not been effectively used to address the issue of plate versus halfspace models.

The recent new analyses of depth and heat flow data [11,16,18–23] have revived interest in the thermal evolution of the lithosphere. Hence, because oceanwide geoid slope estimates should be free of some of the biases associated with fracture zones, we thought it worthwhile to develop techniques to extract the lithospheric cooling signal from such data. Despite the difficulties encountered by the earlier studies, this goal seemed practical given that both improved geoid data [4]

and a digital grid of lithospheric ages [3] are now available. Hence we are able to work with both larger and better datasets than the earlier studies.

3. Analysis

As in the earlier studies (e.g., [36]), we filtered the geoid data to remove the long-wavelength features. By expanding the geoid in spherical harmonic series, we can identify the portions of the geoid for which lithospheric cooling provides the dominant signal. As a check on our conclusions, we performed similar analyses on synthetic ocean-wide geoids predicted from the plate and halfspace models. Though we have explored the global data set, this method of analysis may also be applied to sub-periodic functions over sections of a sphere [39]. We began by expanding the lithospheric age grid and model-predicted geoids in spherical harmonics and comparing them to the spherical harmonic coefficients which define the geoid model [5] derived from observed data. The spherical harmonic expansion of a function is

$$f(\theta,\phi) = \sum_n \sum_m P_{nm} \left[(A_{nm}\cos(m\phi) + B_{nm}\sin(m\phi) \right]$$

where P_{nm} are associated Legendre polynomials and A_{nm} and B_{nm} are the spherical harmonic coefficients. When performing the expansion, regions with no oceanic age (e.g. continental areas) were given a value of zero for the predicted geoid.

The power of a spherical harmonic function is given by

$$S_n = \sum_{n=1}^{m} \left[A_{nm}^2 + B_{nm}^2 \right]$$

The power (Fig. 3A) of the spherical harmonic coefficients for the observed geoid (solid line) decreases rapidly above degree 10, indicating that the data are dominated by longer-wavelength features (e.g., mantle convection). The power of the observed geoid above degree 10 is similar to that predicted for the geoid by either a halfspace (dashed line) or plate (dotted line) model, indicating that the amount of signal present is similar in all three cases.

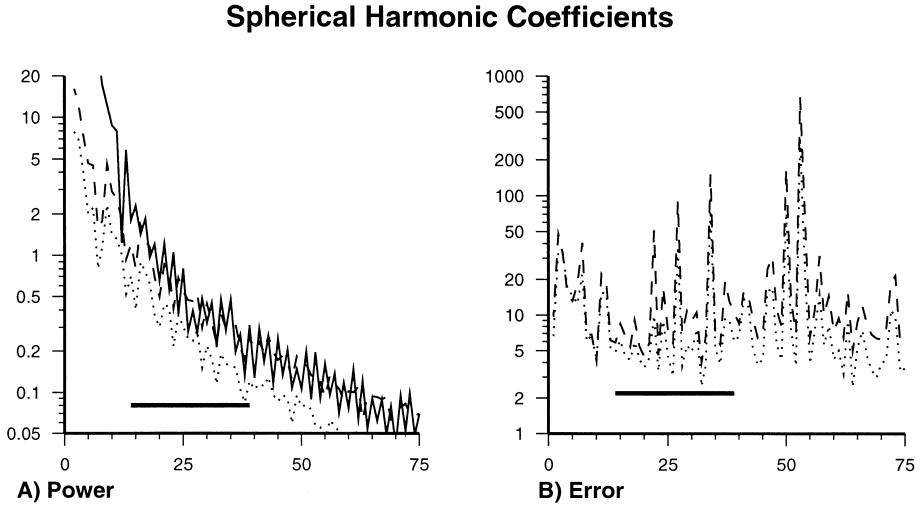

Fig. 3. Spherical harmonic coefficients for the observed and predicted geoids. (A) Comparison of power versus degree for the observed geoid (solid line) and that predicted for the geoid by a halfspace (dashed line) or plate (dotted line) model. (B) Error between the observed geoid and that predicted for the geoid by a halfspace (dashed line) or plate (dotted line) model. The error has a general minimum from degree 14 to 39 (bar), showing that the age-dependent signal is largest at these wavelengths.

We measured the misfit between the predicted and observed geoid signals with the normalized error between two functions

$$E(n) = \sum_n \sum_m \left[\frac{(A_{nm} - \tilde{A}_{nm})^2}{A_{nm}} + \frac{(B_{nm} - \tilde{B}_{nm})^2}{B_{nm}} \right]$$

with spherical harmonic coefficients A_{nm} and B_{nm} and $\tilde{A}_{nm}$ and $\tilde{B}_{nm}$. A lower error indicates that two functions are more similar, whereas a higher error indicates that they are dissimilar [38].

The error (Fig. 3B) between the geoid and the age-predicted signal increases above degree 40 whereas it has a general minimum from degree 14 to 39 (2800–1000 km), showing that the age-dependent lithospheric cooling signal is largest at these wavelengths. The spikes at degrees 24, 27 and 34 may be related to the size of the major ocean basins.

Because the minimum misfit between the two occurs for approximately degrees 14–39, we excluded components outside this range and constructed a filtered geoid using only components 14–39 (Fig. 1C). (A geoid excluding degrees 24, 27 and 34 was also constructed; as the results were not significantly different, we will not discuss it here.) Creation of a geoid using only selected coefficients is equivalent to bandpass filtering the geoid. In order to avoid possible 'ringing', only data more than 1° from the edge of the oceanic basins were used for the geoid slope; this also had the benefit of excluding possible continental influences on the geoid.

The resulting bandpass filtered geoid slope is significantly lower in amplitude (Fig. 1C), but still bears little visual relation to the age data. However, taking the slope of the bandpass filtered geoid, using the method of [36], does much better. The resulting data (Fig. 1D) are visually somewhat similar to the age data. Midocean ridges are visible, and the slope varies away from the ridges. A similar conclusion emerges from comparison of the filtered geoid slope versus age (Fig. 2c) to the geoid slope versus age without spatial filtering (Fig. 2b). The filtering reduces the scatter in the slope data significantly, making the age-dependent signal clearer and hence more suitable for discriminating between lithospheric cooling models.

A quantitative measure of the misfit, c^2, between the observations, y_i, and predicted values, $\hat{y}_i$, is given by

$$c^2 = \frac{1}{N} \sum_{i=1}^{N} \frac{(y_i - \hat{y}_i)^2}{\sigma_{y_i}^2}$$

where $\sigma_{y_i}^2$ is the standard deviation of the observations. To compare the filtering steps, we normalized misfits, dividing that for each model by that found for GDH2. This formulation allows comparison of the misfits between Figs. 2b–d, in which the successive filtering stages reduce the $\sigma_{y_i}^2$. The misfits show that the data are better fit by the two thin-plate models (GDH1, GDH2) than by the thicker-plate (PSM) or halfspace (HS) models.

Although the bandpass filtered geoid slope map (Fig. 1D) looks more like the age map than the geoid or filtered geoid, there clearly are other effects beyond the age dependence. Some of the effects appear to reflect hotspot swells, such as Hawaii. To reduce these effects, we used a window function based on the ratio of geoid to topography, a quantity often used in gravity studies (e.g. [40]). In our application, we used the absolute value of the gradient of the geoid to topography ratio, and excluded values greater than 5 mm km^{-2}. For topography, we used the ETOPO5 dataset, rather than the newer data [24], because the latter derive the topography from the geoid, so their use might introduce some bias. This window function (Fig. 1E) seemed to eliminate many of the swells (Fig. 1F) from the geoid slope map, and hence reduced the scatter in the geoid slope versus age plot (Fig. 2d). The superior fit of the thin-plate models over the halfspace and thick-plate models is thus even clearer. This result is robust to the choice of halfspace model parameters, because slope at young ages is constrained at ~ -15 cm/Ma by the requirement that the thermal model parameters match depth data for young ages. As a result, reasonable halfspace models make similar predictions and do not fit the data as well as a plate model.

After each step, the amount of scatter remain-

ing in the data is reduced, as shown by the decreasing widths of the stippled regions in Fig. 2. This scatter has many possible causes. One may reflect intrinsic variations in lithospheric thermal and crustal structure about their mean values for any age, which cause similar scatter in ocean depth data. Another effect is presumably incomplete removal of the sublithospheric mantle signature. In addition, some of the scatter reflects errors in the age grid: sharp spikes in Fig. 2c,d correspond to the isochrons used by Mueller et al. [3].

The puzzling decrease in geoid slope at young ages may reflect previously observed difficulties with geoid data for young ages [32]. Fracture-zone geoid slope data for ages younger than about 30 Ma are discordant from those for older ages, and are inconsistent with either plate or halfspace thermal models. This problem may in part reflect incomplete removal of partially compensated topography.

4. Conclusions

These results indicate that the geoid can be used as a tool for studying the thermal evolution of oceanic lithosphere. Spatial bandpass filtering and formation of the geoid slope (in itself a spatial filter) can extract the age-dependent signal from the new, high-quality, oceanwide geoid data. This success is gratifying, given that the sublithospheric signal to be removed far exceeds the lithospheric signal sought. Hence although the filtering does not extract a perfect cooling signal, it does quite well. The observation that both oceanwide geoid slope and geoid slope across fracture zones are better fit by a thin-plate model than halfspace and thick-plate models argues that the two data types, each of which is prone to different errors, both record the cooling process with reasonable fidelity. Hence we believe that geoid data provide strong support for the idea of the lithosphere approaching an average equilibrium thermal structure at old ages, as also implied by the depth and heat flow data. Moreover, given that relatively simple processing of oceanic geoid data can provide such useful constraints, we anticipate a renewed interest in analyzing such data, using techniques similar to those used, and using the results to formulate and test models of the thermal evolution of the lithosphere.

Acknowledgements

We thank R.S. Nerem and coworkers, W. Smith and D. Sandwell, and D. Mueller and coworkers for making publicly available the global datasets used here. Portions of the research were conducted by J.E.D. at the NASA Goddard Space Flight Center under the USRA summer research program, with assistance from J. Heirtzler and G. Neumann. The paper has been improved by comments from two anonymous reviewers.*[AC]*

References

[1] C.G. Chase, The geological significance of the geoid, Annu. Rev. Earth Planet. Sci. 13 (1985) 97–117.
[2] S. Solomon, J. Head, Fundamental issues in the geology and geophysics of Venus, Science 252 (1991) 252–260.
[3] R.D. Mueller, W.R. Roest, J.-Y. Royer, L.M. Gahagan, J.G. Sclater, Digital isochrons of the world's ocean floor, J. Geophys. Res. 102 (1997) 3211–3214 (http://omphacite.es.su.oz.au/StaffProfiles/dietmar/Agegrid/agegrid.html).
[4] R.S. Nerem, F.J. Lerch, R.G. Williamson, S.M. Klosko, J.W. Robbins, G.B. Patel, Gravity model improvements using the DORIS tracking system on the SPOT2 satellite, J. Geophys. Res. 99 (1994) 2791–2813.
[5] R.S. Nerem, C. Jekeli, W.M. Kaula, Gravity field determination and characteristics: retrospective and prospective, J. Geophys. Res. 100 (1995) 15053–15074.
[6] W.R. Peltier (Ed.), Mantle Convection, Gordon and Breach, New York, 1989.
[7] B.H. Hager, R.W. Clayton, M.A. Richards, R.P. Comer, A.M. Dziewonski, Lower mantle heterogeneity, dynamic topography, and the geoid, Nature 313 (1985) 541–545.
[8] S. Crough, Geoid anomalies across fracture zones and the thickness of the lithosphere, Earth Planet. Sci. Lett. 44 (1979) 224–230.
[9] D. Turcotte, G. Schubert, Geodynamics: Applications of Continuum Physics to Geological Problems, John Wiley, New York, 1982.
[10] A. Cazenave, Thermal cooling of the lithosphere: new constraints from geoid height data, Earth Planet. Sci. Lett. 70 (1984) 395–406.
[11] A. Cazenave, The geoid and oceanic lithosphere, in: P. Vanicek, N.T. Christou (Eds.), Geoid and Geophysical

Interpretations, CRC, Boca Raton, FL, 1994, pp. 255–284.
[12] M.G. Langseth, X. Le Pichon, M. Ewing, Crustal structure of the mid-ocean ridges, 5, Heat flow through the Atlantic Ocean floor and convection currents, J. Geophys. Res. 71 (1966) 5321–5355.
[13] D.P. McKenzie, Some remarks on heat flow and gravity anomalies, J. Geophys. Res. 72 (1967) 6261–6273.
[14] S.T. Crough, Approximate solutions for the formation of the lithosphere, Phys. Earth Planet. Interact. 14 (1977) 365–377.
[15] B. Parsons, D.P. McKenzie, Mantle convection and the thermal structure of the plates, J. Geophys. Res. 83 (1978) 4485–4496.
[16] M.P. Doin, L.P. Fleitout, Thermal evolution of the oceanic lithosphere: an alternative view, Earth Planet. Sci. Lett. 142 (1996) 121–136.
[17] B. Parsons, J.G. Sclater, An analysis of the variation of ocean floor bathymetry and heat flow with age, J. Geophys. Res. 82 (1977) 803–827.
[18] C.A. Stein, S. Stein, A model for the global variation in oceanic depth and heat flow with lithospheric age, Nature 359 (1992) 123–129.
[19] H.P. Johnson, R.L. Carlson, The variation of seafloor depth with age: a test of existing models based on drilling results, Geophys. Res. Lett. 19 (1992) 1971–1974.
[20] C.A. Stein, S. Stein, Constraints on Pacific midplate swells from global depth-age and heat flow-age models, in: M. Pringle, W.W. Sager, W. Sliter, S. Stein (Eds.), The Mesozoic Pacific, Geophys. Monogr. Ser. Vol. 76, AGU, Washington, DC, 1993, pp. 53–76.
[21] T. Shoberg, C. Stein, S. Stein, Constraints on lithospheric thermal structure for the Indian Ocean from depth and heat flow data, Geophys. Res. Lett. 20 (1993) 1095–1098.
[22] M. Kido, T. Seno, Dynamic topography compared with residual depth anomalies in oceans and implications for age-depth curves, Geophys. Res. Lett. 21 (1994) 717–720.
[23] J. DeLaughter, S. Stein, C.A. Stein, Depth and heat flow anomalies over midplate swells: no unique or exact solution, Eos, Trans. AGU, 79, Spring Meet. Suppl., 1998, p. S210.
[24] W.H.F. Smith, D.T. Sandwell, Global seafloor topography from satellite altimetry and ship depth soundings, Science 277 (1997) 1956–1962 (http://topex.ucsd.edu).
[25] http://www.ngdc.noaa.gov/mgg/sedthick/sedthick.html.
[26] R.S. Detrick, An analysis of geoid anomalies across the Mendocino Fracture Zone: implications for thermal models of the lithosphere, J. Geophys. Res. 86 (1981) 11751–11762.
[27] D.T. Sandwell, G. Schubert, Geoid height-age relation from SEASAT altimeter profiles across the Mendocino fracture zone, J. Geophys. Res. 87 (1982) 3949–3958.
[28] A. Cazenave, B. Lago, K. Dominh, Geoid anomalies over the Northeast Pacific fracture zones from satellite altimeter data, Geophys. J. R. Astron. Soc. 69 (1982) 15–31.
[29] A. Cazenave, B. Lago, K. Dominh, Thermal parameters of the oceanic lithosphere inferred from geoid height data, J. Geophys. Res. 88 (1983) 1105–1118.
[30] M.L. Driscoll, B. Parsons, Cooling of the oceanic lithosphere – evidence from geoid anomalies across the Udintsev and Eltanin fracture zones, Earth Planet. Sci. Lett. 88 (1988) 289–307.
[31] J.C. Marty, A. Cazenave, B. Lago, Geoid anomalies across Pacific fracture zones, Geophys. J. Int. 93 (1988) 1–23.
[32] W.P. Richardson, S. Stein, C. Stein, M.T. Zuber, Geoid data and the thermal structure of the oceanic lithosphere, Geophys. Res. Lett. 22 (1995) 1913–1916.
[33] E. Robinson, B. Parsons, M. Driscoll, The effect of a shallow low-viscosity zone on the mantle flow, the geoid anomalies and geoid and depth-age relationships at fracture zones, Geophys. J. R. Astron. Soc. 93 (1988) 25–43.
[34] P. Wessel, W. Haxby, Geoid anomalies at fracture zones and thermal models for the oceanic lithosphere, Geophys. Res. Lett. 16 (1989) 827–830.
[35] P. Wessel, W. Haxby, Thermal stress, differential subsidence, and flexure at oceanic fracture zones, J. Geophys. Res. 95 (1990) 375–391.
[36] D.T. Sandwell, G. Schubert, Geoid height versus age for symmetric spreading ridges, J. Geophys. Res. 85 (1980) 7235–7241.
[37] C.M. Doucoure, P. Patriat, Thermal diffusivity of the lithosphere derived from altimetry and bathymetry profiles across the Southwest Indian Ridge, Geophys. Res. Lett. 19 (1992) 1543–1546.
[38] G. Balmino, The spectra of the topography of the Earth, Venus and Mars, Geophys. Res. Lett. 20 (1993) 1063–1066.
[39] G.V. Haines, Power spectra of sub-periodic functions, Phys. Earth Planet. Interact. 65 (1991) 231–247.
[40] W.F. Haxby, D.L. Turcotte, On isostatic geoid anomalies, J. Geophys. Res. 83 (1978) 5473–5478.